Clemson University
TigerPrints

Winter 2-1-2008

EXIST'S Gamma-Ray Burst Sensitivity

D. L. Band
CRESSTand Astroparticle Physics Laboratory & Center for Space Sciences and Technology, University of Maryland

J. E. Grindlay
Harvard-Smithsonian Center for Astrophysics

A. Garson III
Washington University

H. Krawczynski
Washington University

Dieter H. Hartmann
Department of Physics and Astronomy, Clemson University, hdieter@clemson.edu

See next page for additional authors

Follow this and additional works at: https://tigerprints.clemson.edu/physastro_pubs

Part of the Astrophysics and Astronomy Commons

Recommended Citation

Please use publisher's recommended citation.

Authors

D. L. Band, J. E. Grindlay, A. Garson III, H. Krawczynski, Dieter H. Hartmann, S. Barthemy, N. Gehrels, and G. Skinner

EXIST'S GAMMA-RAY BURST SENSITIVITY

D. L. Band,[1,2] J. E. Grindlay,[3] J. Hong,[3] G. Fishman,[4] D. H. Hartmann,[5] A. Garson III,[6]
H. Krawczynski,[6] S. Barthelmy,[7] N. Gehrels,[7] and G. Skinner[1,8]

ABSTRACT

We use semianalytic techniques to evaluate the burst sensitivity of designs for the *EXIST* hard X-ray survey mission. Applying these techniques to the mission design proposed for the Beyond Einstein program, we find that with its very large field of view and faint gamma-ray burst detection threshold, *EXIST* will detect and localize approximately two bursts per day, a large fraction of which may be at high redshift. We estimate that *EXIST*'s maximum sensitivity will be ∼4 times greater than that of *Swift*'s Burst Alert Telescope. Bursts will be localized to better than $40''$ at threshold, with a burst position as good as a few arcseconds for strong bursts. *EXIST*'s combination of three different detector systems will provide spectra from 3 keV to more than 10 MeV. Thus, *EXIST* will enable a major leap in the understanding of bursts, their evolution, environment, and utility as cosmological probes.

Subject headings: gamma rays: bursts

1. INTRODUCTION

In its quest to find black holes throughout the universe, the *Energetic X-ray Imaging Survey Telescope* (*EXIST*) will detect, localize, and study a large number of gamma-ray bursts, events thought to result from the birth of stellar mass black holes. We present the methods used to calculate *EXIST*'s capabilities as a gamma-ray burst detector; we use the *EXIST* design evaluated by the National Research Council's "Committee on NASA's Beyond Einstein Program: An Architecture for Implementation"[9] (see also Grindlay 2007). The combination of large detector area, broad energy coverage, and wide field of view (FOV) will result in the detection of a substantial number of bursts with a flux distribution extending to fainter fluxes than that of previous missions. Thus, *EXIST* should detect high-redshift bursts, perhaps even bursts resulting from the death of Population III stars. *EXIST*'s imaging detectors will localize the bursts, while the combination of detectors, both imaging and nonimaging, will result in well-determined spectra from 3 keV to well over 10 MeV.

In this paper we first describe the *EXIST* mission design (§ 2), emphasizing aspects relevant to burst detection. Then we present the sensitivity methodology (§ 3), which we apply to the individual coded mask subtelescopes (§ 4). *EXIST* will consist of arrays of these detectors with overlapping FOVs, and the overall mission sensitivity results from adding the sensitivity of the individual subtelescopes (§ 5). Imaging using counts accumulated over different timescales increases the sensitivity (§ 6). Finally, we combine these different calculations to evaluate *EXIST*'s overall capabilities to study bursts (§ 7).

[1] CRESST and Astroparticle Physics Laboratory, Code 661, NASA Goddard Space Flight Center, Greenbelt, MD 20771; david.l.band@nasa.gov.
[2] Center for Space Sciences and Technology, University of Maryland, Baltimore, MD 21250.
[3] Harvard-Smithsonian Center for Astrophysics, Cambridge, MA 02138.
[4] NASA Marshall Space Flight Center, NSSTC, VP-62, Huntsville, AL 35805.
[5] Clemson University, Clemson, SC 29634.
[6] Washington University, CB 1105, St. Louis, MO 63130.
[7] Astroparticle Physics Laboratory, Code 661, NASA Goddard Space Flight Center, Greenbelt, MD 20771.
[8] Department of Astronomy, University of Maryland, College Park, MD 20742.
[9] Available at http://books.nap.edu/catalog.php?record_id=12006.

2. OVERVIEW OF THE *EXIST* MISSION

The *EXIST* design analyzed here was proposed as the Black Hole Finder Probe for NASA's Beyond Einstein program. In this design, described in Grindlay (2007), the mission consists of two arrays of subtelescopes. The 19 High Energy Telescopes (HETs) will use a cadmium zinc telluride (CZT) detector plane, while the 32 Low Energy Telescopes (LETs) will use a silicon detector plane. The spacecraft will be launched into low Earth orbit (∼500 km) by either an Atlas V-551 (for an orbital inclination of $i \sim 20°$) or a Delta IV 4050H ($i \sim 5°$) for a 5 (minimum) to 10 yr (goal) mission. The CsI active shielding for the CZT detectors will also be instrumented to provide spectral coverage for gamma-ray bursts at higher energies. Table 1 provides the detector parameters relevant to this study. The spacecraft pointing will rock $\pm 15°$ perpendicular to the orbit around the zenith, resulting in nearly uniform sky coverage and sensitivity.

Both the HETs and LETs will image the gamma-ray sky using the coded mask technique. The detector plane "sees" the sky through a mask with open and closed cells that is a fixed distance above the detector plane. Therefore, a source in the FOV casts a shadow with the mask's pattern on the detector plane. The distribution of sources on the sky is deconvolved from the counts detected by the position-sensitive detectors. Sources in the central part of the FOV, the "fully coded" region, illuminate the full detector plane, while sources farther out in the FOV, the "partially coded" region, illuminate only a fraction of the detector plane. The dimensions of the detector plane and mask, as well as the detector-mask distance, determine the FOV, while the detector-mask distance and the dimensions of the mask cells and detector pixels fix the angular resolution.

As for *Swift* and *GLAST*, *EXIST* will run burst detection and localization software on board (the Fast Onboard Burst Alert System [FOBAS]) and telemeter data to the ground for further analysis. In the current design, FOBAS will run both rate and image triggers on the data stream from both the HET and LET subtelescopes. Rate triggers will search for statistically significant increases in the count rates from the subtelescopes. The image triggers will form images from the counts from the individual subtelescopes, add the images, and search the resulting sky image for a new, statistically significant point source. In the current design, images will be formed with 3, 18, 108, 648, and 1296 s

TABLE 1
Parameters of the *EXIST* Detectors

Parameter	High Energy Telescope (HET)	Low Energy Telescope (LET)
Number..	19	32
Detector material..	CZT	Si
Detector thickness (cm).................................	0.5	0.1
Detector plane dimensions (cm)....................	56 × 56	20 × 20
Detector pixels (cm)	0.125	0.02
Mask material	Tungsten	Tungsten
Mask thickness (cm).......................................	0.5	0.05
Mask dimensions (cm)	107.9 × 107.9	40 × 40
Mask pixels (cm)	0.25	0.02
Detector-mask distance (cm)	140	72
Angular resolution (FWHM) (arcmin).........	6.86	1.35
Localization (7 σ, 90% conf.) (arcsec)	<40	<8
Fully coded FOV (deg)	21 × 21	16 × 16
Trigger band ΔE (keV)	10–600, 50–600	3–30
f_{mask}...	0.4	0.4
f_m...	0.737	0.564

accumulation times. When a burst is detected, *EXIST* will down-link the burst time and location (as well as other basic burst parameters) through the Tracking and Data Relay Satellite System (TDRSS) within ∼10–20 s, as is done for *Swift* and will be done for *GLAST*.

Data indicating the time, energy, and pixel of every HET and LET count, as well as other standard science and housekeeping data, will be downlinked approximately every 4 hr through a TDRSS Ku band link, as will be done for *GLAST*. Ground software will calculate more accurate sky positions and other parameters (e.g., durations and spectra) for the bursts detected on board and will search the data stream for bursts that FOBAS did not detect.

The active CsI shields behind the HET detector plane and in the lower part of the HET collimators will be instrumented to provide 64 channel spectra between ∼300 keV and ∼10 MeV (see Garson et al. 2006a). The current plan is that spectra accumulated every 1 s will be downlinked. By buffering the counts from the shields, the count binning will be increased to every 0.1 s for the time period 500 s before to 500 s after the trigger.

3. BURST DETECTION SENSITIVITY

A burst will be detected by *EXIST* when a statistically significant new source is found in either an HET or LET image of the sky. The same criterion applies to *Swift*'s BAT (a single CZT coded mask detector), and therefore the sensitivity analysis we use follows the methodology developed in Band (2003) and applied to the BAT in Band (2006).

Formation of the image in which the burst is detected may be initiated by either a rate or image trigger. A rate trigger will search the count rates from the subtelescopes for a statistically significant increase. An image trigger will search for new sources in images of the sky that will be formed continuously. The new source in an image trigger may not be statistically significant, but will indicate that a burst may be in progress. After either a rate or image trigger, FOBAS (the burst flight software) will vary the time and energy ranges over which counts are accumulated to maximize the signal-to-noise ratio. An image will then be formed from these counts. The threshold for these initial rate or image triggers will be sufficiently loose to allow many triggers; the absence of a statistically significant point source in the final image will weed out the false positives. Note that the final image in which the point source is most significant may be formed from

the counts in a different energy and time bin than that of the counts that initially triggered FOBAS.

Regardless of the process leading to the final image, *EXIST*'s burst sensitivity will be the minimum burst flux that results in a statistically significant point source in an HET or LET image. This is the basis of our analysis. In this section we calculate the sensitivity for a point source in the center of the FOV of a single subtelescope, and in § 5 we consider how this sensitivity varies across the subtelescope arrays' FOV.

G. Skinner (2008, in preparation) derived the source detection sensitivity of a coded mask system when standard assumptions are relaxed: the fraction of the open mask pixels may differ from $\frac{1}{2}$; part of an open mask pixel may be occulted (e.g., by ribs around each pixel to support the *EXIST* masks); the detector pixels may not be small relative to the mask pixels; the source strength may be comparable to the background; and the closed mask pixels may be partially transparent (e.g., at high energy). Here we consider the background-dominated case.

Consider an image formed using counts accumulated over Δt and ΔE. The burst spectrum is $N(E, t)$ (photons cm^{-2} s^{-1} keV^{-1}). Let s be the source flux averaged over Δt and integrated over ΔE. Thus,

$$s = \frac{1}{\Delta t} \int_{\Delta E} dE \int_{\Delta t} dt\, N(E, t). \quad (1)$$

Let the average detector efficiency be

$$\epsilon_0 = \frac{\int_{\Delta E} dE \int_{\Delta t} dt\, \epsilon(E) N(E, t)}{\int_{\Delta E} dE \int_{\Delta t} dt\, N(E, t)}, \quad (2)$$

where $\epsilon(E)$ is the detector efficiency. At high energy photons leak through the closed mask pixels. Define an effective detector efficiency for flux through the closed mask pixels

$$\epsilon_1 = \frac{\int_{\Delta E} dE \int_{\Delta t} dt\, \epsilon(E) N(E, t) e^{-\tau_m(E)}}{\int_{\Delta E} dE \int_{\Delta t} dt\, N(E, t)}, \quad (3)$$

where $\tau_m(E)$ is the optical depth through the closed mask elements. Note that ϵ includes absorption by all material over the entire detector, while $\tau_m(E)$ accounts only for absorption through the closed mask pixels.

For the HETs Garson et al. (2006b, 2006c) find that the photon aperture flux from the cosmic X-ray background (CXB) dominates the background below ∼100 keV, while at higher energy sources such as Earth albedo photons, charged particles, and activation dominate the background. For the LETs the background results primarily from the CXB. The CXB contribution can be modeled semianalytically, while other background sources require complex Monte Carlo calculations. Thus, we model the total background count rate per detector area as

$$
B = (\Delta t)^{-1} \int_{\Delta E} dE \int_{\Delta t} dt
$$
$$
\times \left\{ \epsilon(E) \Phi(E) \Omega_a \left[f_{\mathrm{mask}} + (1 - f_{\mathrm{mask}}) e^{-\tau_m(E)} \right] + b(E) \right\}, \quad (4)
$$

where f_{mask} is the fraction of the mask area that is open, $\Phi(E)$ is the CXB (Gruber 1992), Ω_a is the projected solid angle subtended by the detector's aperture averaged over the detector plane (calculated with the corrected formulae of Sullivan 1971), and $b(E)$ models the other sources of background. The aperture flux includes the leakage of the CXB through the closed mask elements at high energy.

The significance of the burst's image in the background-dominated case is

$$
S_I = f_m s \frac{(\epsilon_0 - \epsilon_1)}{2} \sqrt{\frac{A \Delta t}{B}}, \quad (5)
$$

where A is the detector area and f_m includes the factors resulting from the ribs around the mask pixels, the fraction of the mask pixels that are open, and the finite detector size. For open mask pixels where the ribs cover 0.2 of the pixel area and detector-to-mask pixel ratios of $\frac{1}{2}$ (HET) and 1 (LET), $f_m = 0.737$ and 0.564, respectively.

It is convenient to parameterize the burst flux in terms of

$$
F_T = (\Delta t)^{-1} \int_{\Delta E_0} dE \int_{\Delta t} dt \, N(E, t)
$$
$$
= s \frac{\int_{\Delta E_0} dE \int_{\Delta t} dt \, N(E, t)}{\int_{\Delta E} dE \int_{\Delta t} dt \, N(E, t)}, \quad (6)
$$

where $\Delta E_0 = 1\text{–}1000$ keV.

To understand the effect of transparency through the closed mask pixels, we define the mask factors

$$
g_s = \frac{1 - e^{-\tau_m(E)}}{2} \quad (7)
$$

[relevant to the factor of $(\epsilon_0 - \epsilon_1)/2$] and

$$
g_b = f_{\mathrm{mask}} + (1 - f_{\mathrm{mask}}) e^{-\tau_m(E)} \quad (8)
$$

(relevant to the aperture flux). A decrease in g_s results in a decrease in the detection significance, while an increase in g_b indicates an increase in the aperture flux.

The gamma-ray burst spectrum is modeled using the four-parameter Band function (Band et al. 1993): a low-energy power law with an exponential roll-off [$N(E) \propto E^\alpha \exp(-E/E_0)$] that merges smoothly with a high-energy power law [$N(E) \propto E^\beta$]. The break between the two power laws is characterized by $E_p = (2 + \alpha)E_0$, which is the energy of the maximum of $E^2 N(E) \propto \nu f_\nu$ if $\beta < -2$; i.e., E_p is the photon energy where most of the energy is radiated. We use the flux F_T (photons s^{-1} cm^{-2}) inte-
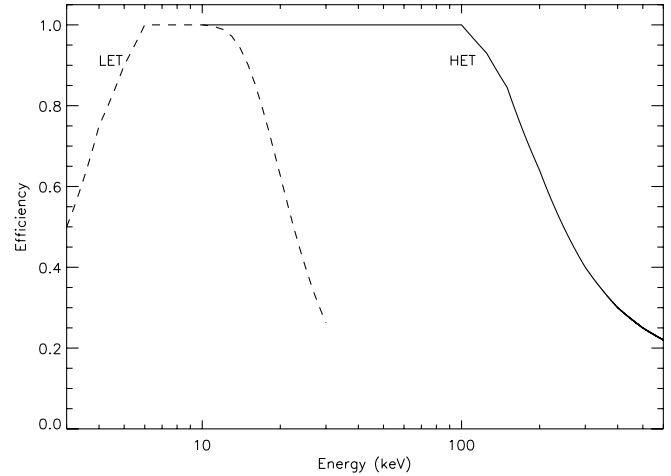

Fig. 1.—Efficiency of the 5 mm thick CZT detectors (*solid line*) and the LET detectors (*dashed line*) as a function of energy.

grated over the 1–1000 keV band to normalize the spectrum (see eq. [6]). Thus, the spectrum is characterized by the normalization F_T, the two spectral indices α and β, and the energy E_p.

Equation (5) can be inverted to find the threshold value of F_T at the peak of the light curve for a given set of the spectral parameters that determine the shape of the burst spectrum: the spectral indices α and β, and the peak energy E_p. The result is a surface in the four-dimensional space given by these spectral parameters; bursts with spectra on one side of this surface (with F_T greater than the value on the surface) will be detected, while bursts on the other side will not. Holding the spectral indices α and β fixed projects this surface into a sensitivity curve in the F_T-E_p plane. The curve also depends on the accumulation time Δt (here $\Delta t = 1$). The dependence of the sensitivity on the accumulation time is discussed below (§ 6).

Note that the threshold value of F_T at a given E_p is *not* the sensitivity of the detector at a photon energy equal to E_p. The power of sensitivity curves in the F_T-E_p plane is that they show the detectability of a burst with a given set of spectral parameters, and thus the sensitivity of different detectors can be compared, regardless of their specific energy response. A CZT-based detector that detects photons in the 10–150 keV band can be compared to a scintillator-based detector that detects photons in the 50–300 keV band.

4. SINGLE SUBTELESCOPE ENERGY SENSITIVITY

4.1. *HET*

A single HET will have a 56 cm × 56 cm (an area of 3136 cm^2) CZT detector plane that is 5 mm thick. The platinum and gold cathode pads on the CZT (∼1000 Å each), the Mylar thermal blankets (two ∼5 mil blankets), and the Kevlar micrometeoroid shield (∼5 mil) in the current design produce negligible absorption >10 keV. Figure 1 shows the efficiency of the CZT detectors as a function of energy.

We calculate the mask factors (eqs. [7] and [8]) using the optical depth through a 5 mm thick, 107.9 cm × 107.9 cm plate of tungsten.[10] Because of the supports necessary for the closed mask pixels, we assume an open fraction of $f_{\mathrm{mask}} = 0.4$. Figure 2 shows the resulting mask factors as a function of energy for both the nominal 5 mm thickness (*solid line*) and a mask with half this thickness (*dashed line*).

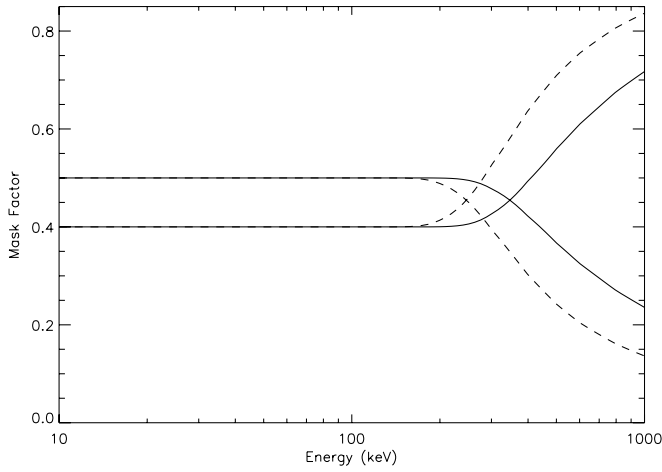[10] See http://physics.nist.gov/PhysRefData/XrayMassCoef/tab3.html.

Fig. 2.—HET mask factors as a function of energy for a tungsten mask that is 5 mm thick (*solid lines*) and 2.5 mm thick (*dashed lines*). The set of curves beginning at 0.4 at low energy is the mask factor g_b (eq. [8]), the fraction of the incident burst flux that reaches the detector plane, whether through an open or closed mask pixel. The set beginning at 0.5 at low energy is the mask factor g_s (eq. [7]), the fraction of burst flux that will be attributed to the burst when an image is formed.

The linear dimensions of the detector and mask pixels will be 0.125 and 0.25 cm, respectively. For a detector-to-mask pixel dimension ratio of 1:2 the factor compensating for the finite size of the detector pixels is $f_m = 0.737$ (see eq. [5]).

The background is modeled (eq. [4]) as the sum of the CXB aperture flux and the continuum background from other sources (for details see Garson et al. 2006b, 2006c). Figure 3 shows the resulting background.

We assume that counts are accumulated over two energy bands $\Delta E = 10-600$ and $40-600$ keV. The $10-600$ keV band is sensitive to soft bursts, where the large number of low-energy burst counts compensates for the large-aperture flux, while the $40-600$ keV band is particularly sensitive to hard bursts where there are sufficient burst photons above 40 keV. The required threshold significance is assumed to be $S_I = 7$ (the same as the BAT's threshold).

Figure 4 shows the sensitivity curve for a single HET subtelescope for three sets of spectral indices and for $\Delta t = 1$ s.
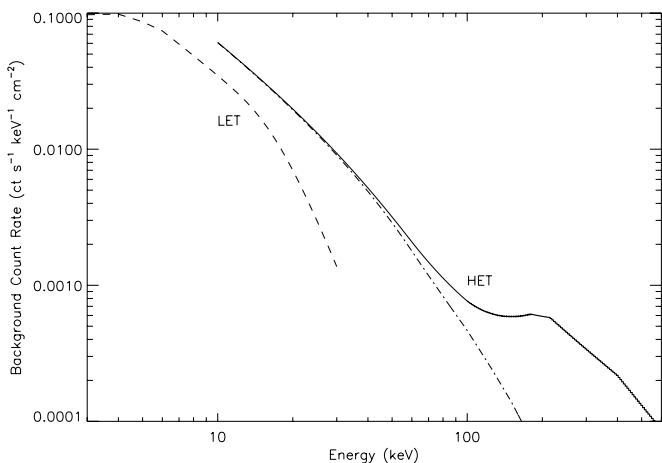

Fig. 3.—Background spectrum for the HETs (*solid and dot-dashed lines*) and LETs (*dashed line*). The CXB aperture flux (*dashed line*: LET; *dot-dashed line*: HET) is based on the parameterization of Gruber (1992), while the total HET background (*solid line*) adds other background components from Monte Carlo simulations (Garson et al. 2006b, 2006c).
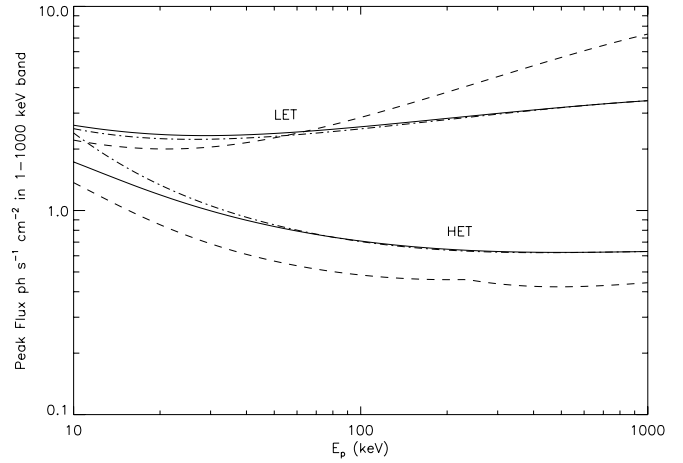

Fig. 4.—Maximum HET (*lower set of lines*) and LET (*upper set of lines*) detection sensitivities for $\Delta t = 1$ s, the threshold peak flux over $1-1000$ keV as a function of the spectrum's E_p. *Solid line*: $\alpha = -1$, $\beta = -2$; *dashed line*: $\alpha = -0.5$, $\beta = -2$; *dot-dashed line*: $\alpha = -1$, $\beta = -3$. Note that this figure shows the sensitivity for detecting a burst with a spectrum characterized by E_p, and not for detecting a photon with an energy equal to E_p.

The survey will localize sources to better than $56''$ (Grindlay 2007). The survey's threshold will be $5\,\sigma$, whereas the burst threshold will be $7\,\sigma$, and typically localization is proportional to $\sim(\sigma - 1)^{-1}$. Thus, we estimate that the HET's localizations will be better than $40''$.

4.2. *LET*

As currently designed, a single LET will have a 20 cm $\times$ 20 cm (an area of 400 cm^2), 1 mm thick Si detector plane with 0.02 cm pixels. Figure 1 also shows the LET efficiency. The mask will be 72 cm above the Si detector plane, with collimators extending from the detector plane to the mask. The 20 cm $\times 20$ cm mask will have a thickness of 0.05 mm and 0.02 cm pixels. Again, because of the need to support the closed mask pixels, we assume an open fraction of $f_{\mathrm{mask}} = 0.4$. Over the LET's energy range ($3-30$ keV) the closed mask pixels will be optically thick. With a mask-to-detector pixel ratio of 1:1, the mask factor in equation (5) is $f_m = 0.564$.

Although we include an internal background of $b(E) = 10^{-5}$ counts cm^{-2} keV^{-1} s^{-1} in our calculation, the background is almost entirely the result of the CXB aperture flux (see Fig. 3).

We assume that a threshold image significance of $S_I = 7$ will be required over a single trigger energy band of $\Delta E = 3-30$ keV. Figure 4 shows the resulting sensitivity. Note that the LETs are less sensitive than the HETs. The slopes of the HET and LET sensitivity curves are consistent with the energy dependence of the LET and HET detectors.

The *EXIST* survey's localizations should be better than $11''$ (Grindlay 2007), and thus accounting for the difference in survey and burst thresholds ($5\,\sigma$ vs. $7\,\sigma$), the LET's burst localizations should be better than $8''$.

5. OFF-AXIS AND MULTIDETECTOR SENSITIVITY

The arrays of HET and LET subtelescopes will each cover a very large total FOV. Any point in these total FOVs will be in the fully or partially coded FOVs of a number of subtelescopes. The resulting multidetector sensitivity across the arrays' FOVs will depend on how the images from the different detectors will be added together; this merging will depend on the exigencies of the available computational power and the required data latency.
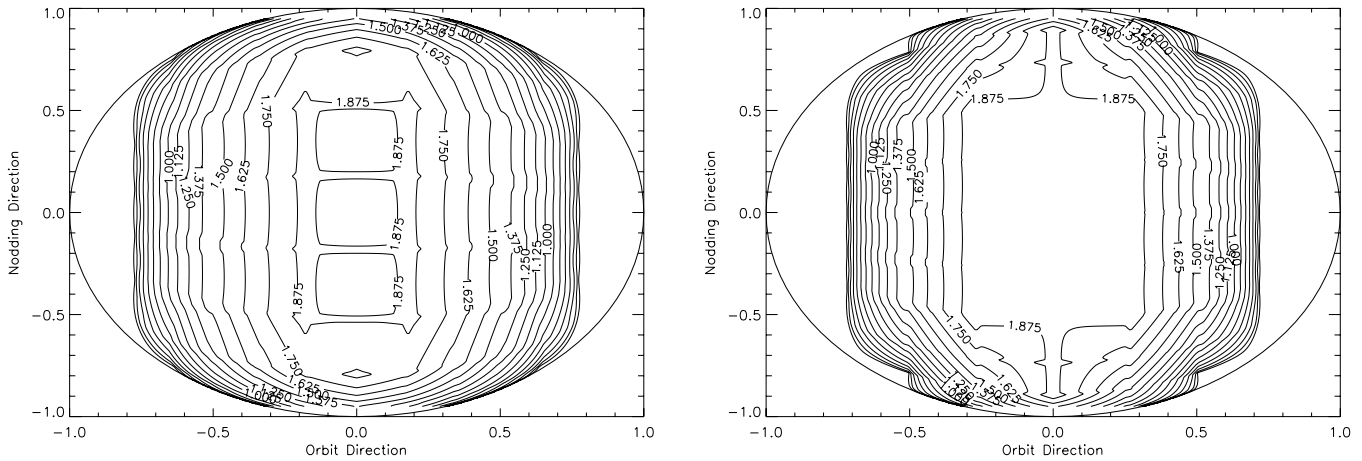
Fig. 5.—Burst detection sensitivity over the sky for the HET (*left*) and LET (*right*) arrays, in units of the sensitivity of a single subtelescope on-axis. Greater sensitivity results in a smaller threshold flux.

Specifically, burst detection and localization on board the *EXIST* spacecraft by radiation-hardened processors will probably be less sensitive than on the ground, where farms of high-speed processors will be available. In addition, localization on board must be rapid so that telescopes on the ground can begin following the burst afterglow.

The calculations above provide the on-axis sensitivity for single HET or LET subtelescopes. Let R be the ratio of the actual sensitivity at a given point in the FOV to this single subtelescope on-axis sensitivity, where sensitivity is proportional to S_I (see eq. [5]) or to the inverse of the threshold peak flux F_T. Thus, larger R means a greater significance for a given peak flux or a smaller threshold peak flux for a given significance.

The source flux falling on the detector plane is only a fraction $f_c \cos \theta$ of the flux it would have on-axis, where f_c is the "coding fraction" that accounts for the partial shadowing of the detector plane by the collimators (the detector sides) and θ is the inclination angle (the angle between the source direction and the detector normal). The nonsource flux that contributes to the background around the source is proportional to the coding fraction f_c. In coded mask imaging only the counts in the region of the detector plane that is not shadowed for a given source contribute to the image around the source. The source flux that impinges on this region is foreshortened by the inclination angle (the "$\cos \theta$" effect), but the background in this region does not depend on the

source's direction. For a single subtelescope the ratio of the off-axis to on-axis significance is therefore $R = f_c^{1/2} \cos \theta$.

The methodology by which the data from multiple detectors will be combined is currently being studied. First, the images can be added. Then the source flux is proportional to $\sum f_{c,i} \cos \theta_i$, the background to $\sum f_{c,i}$, and thus $R_I = (\sum f_{c,i} \cos \theta_i)/(\sum f_{c,i})^{1/2}$. Alternatively, forming images for each subtelescope and adding the significances for the common point sources in quadrature gives $R_Q = (\sum f_{c,i} \cos^2 \theta_i)^{1/2}$. In practice, for the HET and LET arrays the sensitivity over the FOV for these two methods differs very little, and we use R_I.

To calculate the sensitivity over the FOV, we work, and plot results, in a coordinate system that is a projection of the spherical sky directly onto a plane perpendicular to the zenith; i.e., if a point on the sky has the coordinates x, y, z [where $(x^2 + y^2 + z^2)^{1/2} = 1$], then we work in the x-y plane. In this coordinate system, z is along the spacecraft's zenith, x is along the direction of orbital motion, and the spacecraft nods (rocks) in the y-direction. We calculate R_I at different points on this grid.

Figure 5 shows the burst sensitivity over the sky for the HET and LET arrays; the maxima are just under twice the sensitivities (i.e., more sensitive than) of single HET and LET subtelescopes. Figure 6 shows the amount of solid angle at a given sensitivity for both arrays. Thus, different points in the overall FOV will have different sensitivity thresholds, which must be considered when
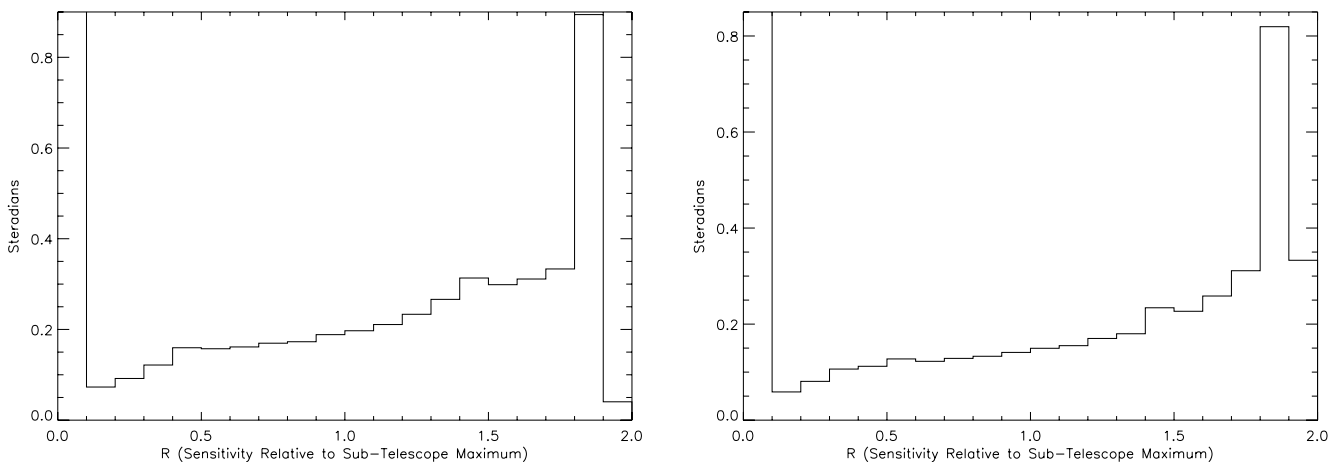

Fig. 6.—Solid angle at a given burst sensitivity for the HET (*left*) and LET (*right*) arrays, in units of a single subtelescope. Greater sensitivity (larger value of R) results in a smaller threshold flux (smaller F_T).

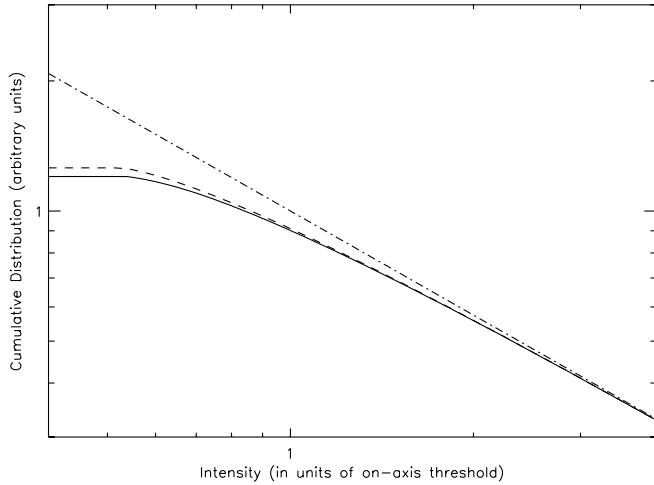FIG. 7.—Effect of the variable detection threshold across the FOV on the cumulative intensity distribution for the HET (*solid line*) and LET (*dashed line*) arrays. The assumed actual distribution (*dot-dashed line*) is a power law with an index of -0.8. The intensity is given in units of the threshold value for a single subtelescope.
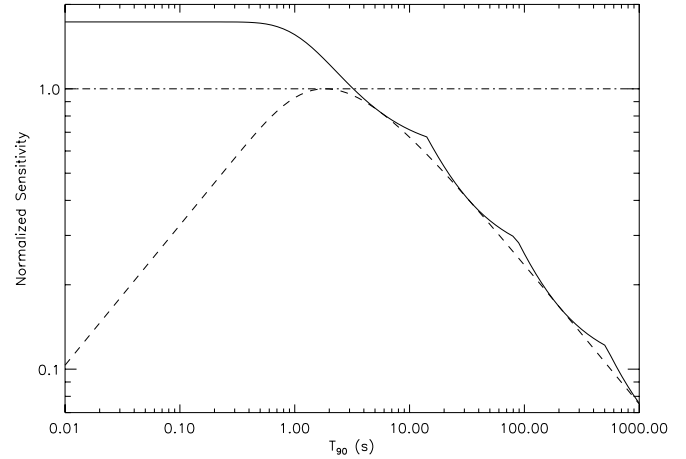

FIG. 8.—Normalized burst sensitivity as a function of burst duration for different accumulation times Δt. The normalized burst sensitivity is the ratio of the peak flux averaged over 1 s for $\Delta t = 1$ s to the peak flux for different Δt values; a smaller value means the detector is more sensitive. The light curve is assumed to be an exponential in time. When a detector system employs more than one Δt, the minimum normalized sensitivity (resulting from the smallest peak flux) is used. The dot-dashed line assumes $\Delta t = 1$, and therefore it is 1 for all durations. The solid line shows the accumulation times currently planned for *EXIST*'s image triggers: $\Delta t = 3, 18, 108, 648,$ and 1296 s. The dashed line assumes all possible values of Δt and thus shows the smallest possible value of the normalized sensitivity.

analyzing the cumulative intensity distribution. Figure 7 shows the low end of the cumulative intensity distribution resulting from variations in the threshold over the FOV; other effects that smooth the threshold are ignored, and therefore the effect demonstrated by this figure applies to any burst intensity distribution. Note that the sensitivity of *Swift*'s BAT also varies over the FOV, affecting the shape of the cumulative fluence or peak flux distributions.

6. DEPENDENCE ON ACCUMULATION TIME Δt

The HET and LET sensitivity curves presented in Figure 4 assumed $\Delta t = 1$ s, i.e., that the bursts were detected in images formed over 1 s. However, modern burst detectors (e.g., *Swift*'s BAT, the *GLAST* Burst Monitor, and *EXIST*) usually use a number of different accumulation times. For an imaging detector the relevant Δt is the accumulation time for the final image. An accumulation time comparable to the burst duration will usually maximize the source significance. A longer accumulation time will dilute the signal with background, reducing the signal-to-noise ratio and therefore the significance of the detection. On the other hand, a shorter accumulation time will often exclude signal that could have increased the significance of the burst detection.

Quantitative analysis of the dependence of burst sensitivity on the accumulation time is difficult because of the large range of burst durations and the great diversity of burst light curves. Some bursts consist of contiguous, overlapping pulses, while others have widely separated pulses. Band (2002) ran a software rate trigger with a wide range of Δt values on the light curves of 100 bright BATSE bursts and determined that using a range of Δt values would increase the burst detection rate by $\sim$25% over the rate for $\Delta t = 1$ s. Band (2006) explained the larger fraction of long-duration bursts relative to short-duration bursts in the *Swift* data set compared to BATSE's as resulting in part from *Swift*'s long accumulation times.

As a demonstration of the increase in sensitivity afforded by using a variety of accumulation times, consider a burst light curve with an exponential shape, $N(t) = N_0 \exp(-t/T)$; the traditional duration of 90% of the emission is $T_{90} = T \ln 10$. In this example the accumulation time is assumed to begin at $t = 0$. Let $F_T(\Delta t)$ be the threshold peak flux averaged over 1 s (this is the quantity plotted in Fig. 4 for $\Delta t = 1$ s) for a given Δt. Then the

ratio of threshold peak fluxes for two different accumulation times Δt_0 and Δt_1 is

$$\frac{F_T(\Delta t_1)}{F_T(\Delta t_0)} = \sqrt{\frac{\Delta t_1}{\Delta t_0}} \frac{1 - \exp(-\Delta t_0/T)}{1 - \exp(-\Delta t_1/T)}. \qquad (9)$$

If a detector uses a set of Δt values, then the smallest value of $F_T(\Delta t)$ should be used for any given value of T. We assume that we are in the background-dominated case (eq. [5]); the detectability of very short bursts might be limited by a paucity of source counts.

Figure 8 shows this ratio for $\Delta t_0 = 1$ s and different sets of Δt_1. Thus, this figure shows how the sensitivity of a mission such as *EXIST* to short- and long-duration bursts is increased by using a variety of accumulation times. The dashed line assumes $\Delta t_1 = 1$ s, and thus the ratio is equal to 1. Currently *EXIST*'s planned imaging trigger (which is *not* the final imaging step in *EXIST*'s burst detection process) will use $\Delta t_1 = 3, 18, 108, 648,$ and 1296 s; this is shown by the solid line. Finally, Δt_1 may be varied to maximize the signal-to-noise ratio, minimizing $F_T(\Delta t_1)$ to the smallest possible value; this is shown by the dot-dashed line.

If burst light curves could be described by the exponential shape of this example (and bursts did not undergo spectral evolution, which makes the duration energy dependent), then the HET or LET threshold peak flux of a burst of a given peak energy E_p and duration T_{90} would be the product of F_T from Figure 4 and the ratio from Figure 8.

We emphasize that this is a highly idealized example meant to demonstrate how the variable accumulation times of *EXIST*'s burst detection system will increase the sensitivity to long- and short-duration bursts. This is particularly relevant to high-redshift bursts whose durations will be time dilated.

7. DISCUSSION

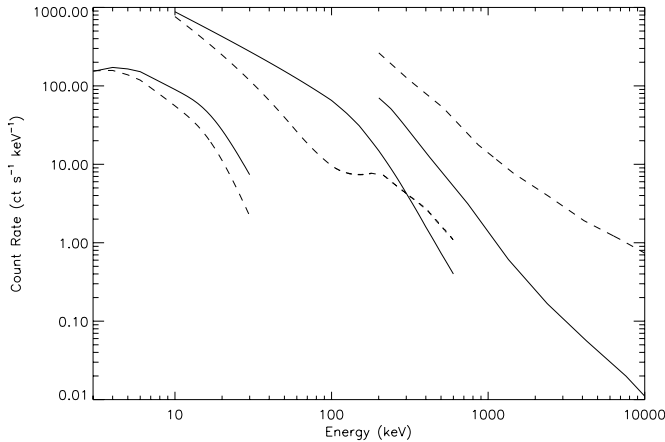From the preceding analysis, we can draw several conclusions on *EXIST*'s impact on the study of gamma-ray bursts.

FIG. 9.—Source count (*solid lines*) and background (*dashed lines*) spectra for the LETs (*left-hand set of lines*), HETs (*middle set of lines*), and CsI shields (*right-hand set of lines*). The burst spectrum has $\alpha = -1$, $\beta = -2$, $E_p = 300$ keV, and $F_T = 7.5$ photons cm^{-2} s^{-1}. Based on the subtelescopes' FOVs in the current design, we assume that spectra can be formed from the equivalent of four HET and LET subtelescopes and the shields of nine HET subtelescopes.

First we estimate the *EXIST* burst detection rate. The BATSE observations provide the cumulative burst rate as a function of the peak flux value ψ_B averaged over $\Delta t = 1$ s in the $\Delta E = 50-300$ keV band (Band 2002):

$$N_B \sim 550 \left(\frac{\psi_B}{0.3 \text{ photons cm}^{-2} \text{ s}^{-1}} \right)^{-0.8} \text{ bursts yr}^{-1} \text{ sky}^{-1}. \tag{10}$$

The HET threshold sensitivity for a single subtelescope on-axis is $\psi_B \sim 0.12$ photons cm^{-2} s^{-1} for $E_p > 100$ keV. Using the BATSE rate in equation (10) and integrating over the solid angle distribution in Figure 6 gives a burst detection rate for the HET of $\sim$400 bursts yr^{-1}. Note that this rate is over the BATSE-specific values of ΔE and Δt, and *EXIST* will use at least two different values of ΔE (see § 4.1) and a variety of Δt values (see § 6). Consequently, this rate should be increased by approximately 50% to account for the soft, faint, long-duration bursts to which BATSE was less sensitive than *EXIST*'s HET will be; we therefore expect the HET array to detect $\sim$600 bursts yr^{-1}.

The value of ψ_B for an LET varies more with the burst spectral parameters than for an HET, and therefore estimates of the LET burst detection rate based on the BATSE rate are much more uncertain. For a single LET $\psi_B \sim 0.3$ photons cm^{-2} s^{-1} on-axis at $E_p = 100$ keV, which gives a burst detection rate of $\sim$180 bursts yr^{-1} using equation (10) and the LET distribution in Figure 6. This rate should be increased by a factor of 2 to account for the different energy band ΔE and accumulation times Δt. We use a larger adjustment factor for the LETs than for the HETs because the LETs' energy band will overlap less with BATSE's than the HETs'. We therefore expect the LET array to detect $\sim$350 bursts yr^{-1}.

Next we simulate the spectra that the *EXIST* suite of detectors will observe. Figure 9 shows a count spectrum (counts s^{-1} keV^{-1}) for a moderately strong burst as it might be observed by the LETs (*left-hand set of lines*), HETs (*middle set of lines*), and the CsI active shields for the HETs (*right-hand set of lines*; based on Garson et al. 2006a). The solid lines show the signal count rate, while the dashed lines provide the estimated background. Thus, *EXIST* will facilitate spectral-temporal studies.
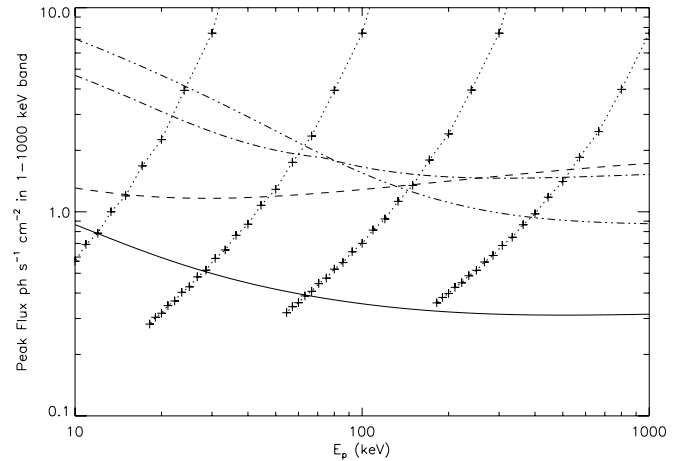

FIG. 10.—Maximum detector sensitivity for HET (*solid line*), LET (*dashed line*), *Swift*'s BAT (*dot-dashed line*), and BATSE's LAD (*double-dot–dashed line*) assuming $\Delta t = 1$ s, $\alpha = -1$, and $\beta = -2$. The HET and LET sensitivities assume burst detection by multiple subtelescopes. Also shown are tracks for identical bursts at different redshifts. The bursts have different E_p and $F_T = 7.5$ photons cm^{-2} s^{-1} when at $z = 1$. The points on the track are spaced by $\Delta z = \frac{1}{2}$; the faintest bursts on each track are at $z = 10$. Burst pulses are assumed to narrow by $E^{-0.4}$. The assumed cosmology is $\Omega_m = 0.3$ and $\Omega_\Lambda = 0.7$ (H_0 is irrelevant to this calculation).

Particularly important to physical burst emission models is determining E_p, which is typically of order 250 keV (Kaneko et al. 2006). In addition, correlations of E_p with other burst properties, such as the "isotropic" energy (the Amati relation; Amati 2006) or total energy (the Ghirlanda relation; Ghirlanda et al. 2004), have been proposed. "Pseudoredshifts" calculated from the observables related to the burst-frame parameters in these relations can be used in burst studies when spectroscopic redshifts are not available and can guide ground observers in allocating telescope time to observing potential high-redshift bursts. The recently proposed Firmani relation (Firmani et al. 2006) correlates E_p, the peak luminosity, and a measure of the burst duration, all of which are related to observables in the gamma-ray band. Thus, pseudoredshifts will be estimated using the Firmani relation based on *EXIST* data alone, independent of observations by other facilities.

With well-determined broadband spectra down to 3 keV, *EXIST* will be capable of determining whether the Band function (Band et al. 1993) suffices to describe burst spectra. For example, Preece et al. (1996) found evidence in the BATSE data for the presence of additional emission below 10 keV.

By scaling from the *EXIST* survey's source localization (Grindlay 2007), we find that bursts should be localized at threshold by the HETs and LETs to better than 40″ and 8″, respectively; this localization should scale as $\sim (\sigma - 1)^{-1}$. Because the HETs are more sensitive to the LETs, the HET localization is relevant to the faintest bursts *EXIST* will detect.

EXIST's burst capabilities calculated above will constitute a major leap beyond current detectors and should increase the number of high-redshift bursts detected. On average, high-redshift bursts should be fainter, softer, and longer than low-redshift bursts (although the broad burst luminosity function and great variety in burst light curves and spectra obscure this trend). Figure 10 compares the detector sensitivities of the HET (*solid line*) and LET (*dashed line*) arrays to the BAT on *Swift* (*dot-dashed line*) and BATSE's Large Area Detector (LAD; *double-dot–dashed line*). As discussed above, the sensitivity is the threshold peak flux F_T integrated over the 1–1000 keV band as a function of the

spectrum's E_p; $\alpha = -1$ and $\beta = -2$ are assumed. In addition, the figure shows families of identical bursts at different redshifts (*lines with plus signs*). Each family is defined by the value of E_p in the burst frame; here again $\alpha = -1$ and $\beta = -2$ are assumed. In each family the burst would be observed to have $F_T = 7.5$ photons cm^{-2} s^{-1} if it were at $z = 1$. The points marked by plus signs are spaced every $\Delta z = \frac{1}{2}$; thus, the uppermost points are at $z = 1$ and the lowermost points are at $z = 10$. The pulses in burst light curves become narrower (shorter) at higher energy, an effect that is generally proportional to $E^{0.4}$ (Fenimore et al. 1995). Since the observed light curve originated in a higher energy band, pulses should become narrower with redshift, reducing the peak flux when integrated over a fixed accumulation time; the plotted families include this effect. Finally, in § 6 we showed that forming images on long timescales increases the sensitivity to long-duration bursts, as might result from cosmological time dilation.

8. SUMMARY

We presented our method for analyzing the gamma-ray burst sensitivity of *EXIST* and applied it to the design for the Beyond Einstein program; this methodology will be used to guide and evaluate the evolving mission design. With two arrays of coded mask detectors covering the 3–30 keV (Si) and 10–600 keV (CZT) bands and nonimaging high-energy CsI detectors (0.2–10 MeV), *EXIST* will be a significant gamma-ray burst observatory. *EXIST* will detect and localize ∼2 bursts per day, observing their spectra from 3 keV to over 10 MeV. For bursts with comparable spectra and light curves *EXIST* will be approximately 4 times more sensitive than *Swift*'s BAT with a much larger FOV. With these capabilities, *EXIST* will accumulate a large sample of bursts with well-determined properties such as E_p and redshift, facilitating physical modeling and population studies, and realizing the potential of gamma-ray bursts as cosmological probes.

REFERENCES

Amati, L. 2006, MNRAS, 372, 233
Band, D. 2002, ApJ, 578, 806
———. 2003, ApJ, 588, 945
———. 2006, ApJ, 644, 378
Band, D., et al. 1993, ApJ, 413, 281
Fenimore, E. E., in't Zand, J. J. J. M., Norris, J. P., Bonnell, J. T., & Nemiroff, R. J. 1995, ApJ, 448, L101
Firmani, C., Ghisellini, G., Avila-Reese, V., & Ghirlanda, G. 2006, MNRAS, 370, 185
Garson, A., III, Krawczynski, H., Grindlay, J., Fishman, G. J., & Wilson, C. A. 2006a, A&A, 456, 379
Garson, A., III, Krawczynski, H., Weidenspointner, G., Novikova, E. I., Grindlay, J., Hong, J., & Jung, I. V. 2006b, Proc. SPIE, 6319, 9

Garson, A., III, Krawczynski, H., Weidenspointner, G., Novikova, E. I., Grindlay, J., Hong, J., & Jung, I. V. 2006c, preprint (astro-ph/0610049)
Ghirlanda, G., Ghisellini, G., & Lazzati, D. 2004, ApJ, 616, 331
Grindlay, J. 2007, in AIP Conf. Proc. 921, The First GLAST Symposium (New York: AIP), 211
Gruber, D. E. 1992, in The X-Ray Background, ed. X. Barcons & A. C. Fabian (Cambridge: Cambridge Univ. Press), 44
Kaneko, Y., Preece, R. D., Briggs, M. S., Paciesas, W. S., Meegan, C. A., & Band, D. L. 2006, ApJS, 166, 298
Preece, R. D., Briggs, M. S., Pendleton, G. N., Paciesas, W. S., Matteson, J. L., Band, D. L., Skelton, R. T., & Meegan, C. A. 1996, ApJ, 473, 310
Sullivan, J. D. 1971, Nucl. Instrum. Methods, 95, 5